Measurement Approaches to Develop a Fundamental Understanding of Scratch and Mar Resistance

Mark R. VanLandingham[†,a] Neng-Kai Chang[b], Tsun Yen Wu[b], Li-Piin Sung[a,d], Vincent D. Jardret[c], and Shuo-Hung Chang[b]

[a]*National Institute of Standards and Technology*
Gaithersburg, MD 20899

[b]*Department of Mechanical Engineering, National Taiwan University*
Taipei, Taiwan, R.O.C.

[c] *Tribometrix, Inc, Knoxville, TN 37918*

[†] Current address: *Army Research Laboratory, Aberdeen Proving Ground, MD 21005*
[d]Address all correspondence to this author; email: lipiin@nist.gov

Abstract

Instrumented indentation and confocal microscopy were used to characterize the surface mechanical response of polymeric materials. Viscoelastic behavior was measured using instrumented indentation. A model based on contact between a rigid probe and a viscoelastic material was used to calculate values for creep compliance and stress relaxation modulus for two polymeric materials, epoxy and poly(methyl methacrylate) or PMMA. Scratch testing was performed on these materials with various probes under a variety of conditions, and confocal microscopy was used to characterize the resulting deformation. Relationships between viscoelastic behavior, scratch damage and appearance are currently being explored using these methods along with finite element modeling.

I. INTRODUCTION

Scratch and mar resistance is an important characteristic for polymeric materials and coatings in a wide variety of applications. Many surface mechanical test methods, some standardized through groups such as ASTM International, some standardized within a particular company, and others that are ad hoc standards, have been used with limited success and primarily for qualitative comparisons and quality assessment purposes. Field simulation tests have been developed based on service conditions that can cause scratching and marring of a polymer that generally involve either wet abrasion using abrasive slurries or dry abrasion using abrasive powders or papers [1-5]. All of these tests produce relative measures of scratch resistance, usually based on mass loss, visual inspection, gloss changes, or changes in gray scale level or ΔL, often with poor repeatability and/or reproducibility. To produce measurable changes in such metrics, the severity of test conditions in terms of applied force or duration of test, for example, can be so drastic as to induce abnormal damage mechanisms producing misleading results [6].

Recent efforts have been aimed at measuring quantitative material properties and understanding relationships between surface properties and performance characteristics. In most of these studies, single-probe testing devices [3-22], including instrumented indentation and scratch

systems [4-6, 17-19] and atomic force microscopes [3, 20-22], have been used to simulate single asperity contact, as opposed to multi-asperity contact associated with the field simulation tests. Single-probe scratch testing can be useful for characterizing time and strain dependent behavior of a polymeric material under a number of contact conditions [9]. However, an inappropriate choice of tip geometry and loading conditions can still produce damage that is much more severe than in-service damage [4, 23].

Scratch and mar resistance is most often characterized using appearance metrics. Currently, however, relationships between appearance attributes and surface deformation associated with scratching and marring are ambiguous. This lack of connectivity is one of the major barriers to the development and acceptance of a unified standard or set of standards for determining scratch and mar resistance. Another major barrier is the specification of testing conditions. Test variables, such as tip geometry, scratch speed, and applied load, differ from one study to another, sometimes by orders of magnitude. These large variations are even associated with studies in which relatively similar single-probe devices have been used. Because scratch and mar behavior is related to both the surface properties of the material and the loading conditions, laboratory testing should provide an understanding of how the material will perform under a wide variety of conditions. In particular, effects of temperature, strain and strain rate, which are related to the material properties, the probe geometry, the loading rate, and the scratch speed, should be thoroughly investigated. To date, only Briscoe et al. [8-12], and more recently Sue and co-workers [16, 17] and Gauthier et al. [24, 25], have studied the effects of different test variables on the scratch behavior of polymers. Also, very little modeling has been performed to understand how changes in testing conditions affect the local stress and strain fields [26, 27]. Because of these deficiencies, relationships between polymer properties and scratch and mar resistance are not well understood.

In this paper, an instrumented indentation and scratch system is used along with confocal microscopy to characterize the surface mechanical response of polymeric materials. Indentation versions of creep and stress relaxation tests are first used to study the viscoelastic behavior of two polymeric materials, epoxy and poly(methyl methacrylate) or PMMA. A model based on contact between a rigid probe and a viscoelastic material was used to calculate values for creep compliance and stress relaxation modulus as functions of time and loading conditions. Scratch testing was then performed with the indentation and scratch instrument on these materials with various probes under a variety of conditions, and confocal microscopy was used to characterize the resulting deformation. Relationships between viscoelastic behavior, scratch damage and appearance are currently being explored using these methods along with finite element modeling that incorporates the constitutive behavior measured using the instrumented indentation results.

II. EXPERIMENTAL METHODS AND MATERIALS[1]

A. Materials

Materials used in this study included an amine-cured epoxy and PMMA. Epoxy films approximately 190 μm in thickness were cast onto silicon wafers in a CO_2-free and H_2O-free

[1] Certain commercial instruments and materials are identified in this paper to adequately describe the experimental procedure. In no case does such identification imply recommendation or endorsement by the National Institute of Standards and Technology, nor does it imply that the instruments or materials are necessarily the best available for the purpose.

glove box using a drawdown technique. Highly pure diglycidyl ether of bisphenol A with a mass per epoxy equivalent of 172 g and 1,3-bis(aminomethyl)-cyclohexane were mixed at the stoichiometric ratio. All epoxy samples were cured at room temperature for 48 h, followed by post-curing at 130 ºC for 2 h. The films were then removed from the silicon substrates by immersion in warm water followed by peeling with tweezers. The glass transition temperature, T_g, of the cured films was (123 ± 2) ºC, as estimated using dynamic mechanical analysis. PMMA film samples with approximate thickness of 3.8 mm were provided directly from a commercial source. Fused silica, supplied by MTS Systems Inc., was used as a reference material (nominal elastic modulus, E = 75 GPa) for tip shape determination via indentation.

B. Instrumented Indentation

Instrumented indentation was performed using a NanoIndenter XP and a NanoIndenter DCM (MTS Systems, Inc.). Forces applied using the XP system, in general, ranged from 0.2 mN to 100 mN, while those applied using the DCM system ranged from 0.01 mN to 10 mN. For measurements made with the XP system, several different probe tip shapes were used, including a Berkovich pyramid, and two rounded cones with semi-apical angles of 45º and tip radii of 1.5 µm and 10 µm, respectively (tip angles and radii are nominal values provided by the manufacturer). Only a Berkovich tip was available for testing with the DCM system. Tip shape has been measured for these probes using indentation of fused silica and by directly imaging the probes with an atomic force microscope (AFM), as detailed elsewhere [28]. Indentation creep response was measured using step loading to a prescribed force, P_0, which was then held for 100 s. Indentation relaxation response was measured using a step displacement to a depth, h_0, related to a prescribed load. This depth was then held for 100 s. These test methods are detailed elsewhere [29].

C. Scratch Testing

Scratch testing was performed using the NanoIndenter XP described previously. Several different probe tip shapes were used, including the two rounded conical probes described previously. Results presented in the following section are for the 1.5 µm radius cone and a similar 1.0 µm radius cone (also with a 45º semi-apical angle). Testing parameters used included scratch lengths of 250 µm and 1 mm and scratch velocities of (2, 10, 50 and 250) µm/s. Initially, a progressive-force scratch method was used in which the applied force was increased linearly with scratch distance from a very low force (nominally 20 µN) at the beginning of the scratch to approximately 100 mN at the end of the scratch. These tests were followed by constant-force scratch testing at force levels ranging from 2 mN to 40 mN, depending on the sample and the force levels at which changes in deformation behavior were observed during the progressive-force tests. Regardless of the type of test, a profile of the surface was first performed using a small contact force of 20 µN, followed by the scratch test and then by a post scratch profile again using a 20 µN contact force; both profiles and the scratch test were performed along the same path.

D. Optical Characterization

Optical characterization using a Ziess model LSM510 reflection laser scanning confocal microscope (LSCM) was employed to characterize the surface morphology of scratches produced using the NanoIndenter XP. The LSCM utilizes coherent light and collects light exclusively from a single plane (a pinhole sits conjugated to the focal plane) and rejects light out of the focal plane. The wavelength, numerical aperture (N.A.) of the objective, and the size of

the pinhole dictate the resolution in the thickness or axial direction [30]. By moving the focal plane, single images (optical slices) can be combined to build up a three dimensional stack of images that can be digitally processed. In this paper, all LSCM images are presented as two dimensional intensity projections resulting from a series of overlapping optical slices (a stack of z-scan images) with a z-step of 0.1 μm. The laser wavelength used was 543 nm.

III. RESULTS AND DISCUSSION

A. Instrumented Indentation

The rheological behavior of viscoelastic materials, such as polymers, is typically characterized as a function of various test conditions, including the levels of stress and strain, the strain rate, and the temperature. Indentation measurements, however, are based on force and displacement rather than stress and strain, such that comparisons with traditional mechanical and rheological measurements are difficult. Additionally, properties are determined from instrumented indentation using analyses and loading histories developed for elastic and elasto-plastic materials, i.e., time dependence is neglected. To better assess the indentation response of polymeric materials, a mathematical analysis of quasi-static contact between a rigid axisymmetric indenter and a linear viscoelastic solid was used [31]. Values of creep compliance, $J(t)$, and stress relaxation modulus, $G(t)$, in shear were estimated using relatively simple loading histories. For indentation creep, a force P_0 was applied at time $t = 0$ and held constant, and $J(t)$ was calculated from measurements of P_0 and variables related to the contact geometry, such as contact area, $A(t)$, and penetration depth, $h(t)$. Examples of such relationships are given by Eq. (1) and Eq. (2) for a paraboloidal (spherical) indentation tip of radius R and for an ideal by conical (pyramidal) tip of semi-apical angle θ, respectively:

$$J(t) = \frac{8h(t)\sqrt{A(t)/\pi}}{3P_0} \tag{1}$$

$$J(t) = \frac{A(t)\tan\theta}{P_0} \tag{2}$$

Similarly, an analogue to stress relaxation was achieved by applying a displacement h_0 at $t = 0$ and holding it constant, yielding values of relaxation modulus, $G(t)$, determined from measured values of h_0, the corresponding contact area, A_0, and the force, $P(t)$. Examples of these relationships are given by Eq. (3) and Eq. (4) for a paraboloidal (spherical) indentation tip of radius R and for an ideal by conical (pyramidal) tip of semi-apical angle θ, respectively:

$$G(t) = \frac{3P(t)}{8h_0\sqrt{A_0/\pi}} \tag{3}$$

$$G(t) = \frac{P(t)}{A_0\tan\theta} \tag{4}$$

The extensional relaxation modulus, *E(t)*, was calculated from *G(t)* using the following approximation for homogeneous, isotropic, elastic materials, and assuming that Poisson's ratio, ν, is independent of time:

$$E = 2G(1+\nu) \tag{5}$$

Examples of force and displacement histories for these types of tests are shown in Fig. 1, and the resulting values of *J(t)* and *E(t)* are shown for the epoxy and PMMA materials in Fig. 2 and Fig. 3, respectively. Indentation data in each of these figures were generated using Berkovich pyramidal tip geometry. Values of *E(t)* measured using a tensile rheometer (see Ref. 29 for more details) are also shown in Fig. 2 and Fig. 3 for comparative purposes. Qualitatively, the indentation data appears to be consistent with behavior expected of glassy epoxy and PMMA polymers – compliance values are on the order of 10^{-9} Pa and trend higher with increasing time and increasing force, while relaxation modulus values are on the order of 10^{9} Pa and trend lower with increasing time and increasing displacement. However, in all cases, values of *J(t)* and *E(t)* were dependent upon the level of stress (force) or strain (displacement). From the tensile rheometry data, values of *E(t)* measured for epoxy were similar for strain levels of 0.01 % and 0.1 %. The application of a 1 % strain, however, resulted in significantly lower relaxation modulus values. For PMMA, differences in *E(t)* were observed between strain levels of 0.01 % and 0.1 %, where the increase in strain again resulted in lower values of *E(t)*. Similar behavior was observed in the indentation results, although in some cases, the data scatter obscured the trends. In general, increases in the displacement applied in an indentation relaxation experiment resulted in lower relaxation modulus values. Also, increases in the constant load applied in an indentation creep experiment resulted in higher values of creep compliance. Keeping in mind the uncertainties related to tip shape at low loads and displacements, the slope or curvature of the *J(t)* and *E(t)* double logarithmic data appears to remain relatively constant with increasing force or displacement for a given set of tests, suggesting separability of the time-dependent behavior from the stress- or strain-dependent behavior. The large differences between values of *E(t)* for indentation compared to tensile rheometry could be an indication of the strain dependence coupled with the large strains expected local to the Berkovich tip relative to the strains applied by the rheometer. Also, the behavior under a multi-axial state of strain could be significantly different compared to behavior under uni-axial strain.

To estimate the stresses and strains applied in an indentation measurement, a number of relationships have been suggested. Indentation hardness, *H*, is also the mean stress or pressure in an indentation experiment, i.e., it is the ratio of force, *P*, to contact area, *A*, where *A* is in general related to displacement, *h*, by the tip geometry. For a spherical or paraboloidal tip, indentation strain, $\bar{\varepsilon}$, is related to the ratio of the contact radius, *r*, to the tip radius, *R*, where *r* is a function of *h* [32, 33]. For conical or pyramidal tip geometry, a nominal indentation strain is related to the characteristic included angle, θ, of the tip. Analyses by Tabor [34] that were empirically based and in which ideal plastic behavior was assumed can be used to generate the following two equations for $\bar{\varepsilon}$ for ideal paraboloidal and Berkovich tip geometries, respectively:

$$\bar{\varepsilon} = 0.2r/R \tag{6}$$

$$\bar{\varepsilon} = 0.25\cot\theta \tag{7}$$

For example, Tabor estimated the representative strain for a Berkovich tip to be between 8 % and 10 %, and Eq. (7) yields a value of 8.9 % for an ideal Berkovich tip (θ = 70.32º). Note that relationships similar to Eq. (2) and Eq. (4) were recently derived for pyramidal indenters [33] directly from Hook's law by assuming P / A as a representative stress and $(\cot \theta)\bullet(dh / h)$ as a representative strain increment. For any tip geometry, the indentation strain rate can be calculated from the ratio $\dot{h}/h$, where $\dot{h}$ is the rate of change of h with time, t, or $\dot{h} = dh/dt$.

In Fig. 4a, values of *J(t)* are shown for epoxy indented with the XP system using a rounded conical tip with a 10 μm tip radius and a Berkovich tip. In Fig. 4b, effective strains, calculated using Eq. (6) and Eq. (7) for these rounded conical and Berkovich tip shapes, respectively, are plotted as a function of displacement. Tip shape analysis, described in detail in Ref. 28, was used to determine an effective conical angle, θ, for the Berkovich tip of approximately 71.1º and an effective radius function, R_{eff}, for the rounded conical tip, which were then used in the calculation of effective strain. The effective strain and the corresponding creep compliance values are lower for the rounded conical tip compared to the Berkovich tip for all tests except the two highest loads, 10 mN and 20 mN. At these two loads, the effective strain levels and the creep compliance values for the rounded conical tip are similar to those for the Berkovich tip, i.e., in the range of 8 % to 10 %. Also, the larger variation in creep compliance for the rounded conical tip with load appears to reflect the larger expected changes in the associated effective strain compared to the Berkovich tip, for which a smaller variation in creep compliance with load was observed, possibly in response to a small variation in effective strain related to deviations in the actual tip geometry from the ideal case plotted in Fig. 4b. Regarding the stress relaxation modulus data (see Fig. 2a and Fig. 3a), nonlinear viscoelastic analysis in which time-temperature-strain superposition is assumed could be used to vertically shift the data as a function of strain level. The large amount of vertical shifting necessary would then indicate much larger effective strains in the indentation measurements relative to the rheology measurements. Because the relationships between indentation parameters and stress and strain, such as Eq. (6) and Eq. (7), are based on elastic or elastic-plastic behavior, further investigations are needed to quantify the effective stress and strain levels as a function of indentation tip geometry for viscoelastic materials.

B. Characterization of Scratch Behavior

From the results of the indentation testing, the behavior of polymers under "single asperity" contact loading appears to be characteristic of nonlinear viscoelasticity. Because of the intense stresses and strains local to the tip-sample contact during a scratch event, characterizing nonlinear mechanical behavior of polymeric materials is important for relating material properties to scratch and mar resistance. The use of properties measured under linear viscoelastic conditions could be quite different compared to those measured under nonlinear viscoelastic conditions, thus resulting in poor predictive capabilities. Thus, instrumented indentation provides a means for measuring nonlinear behavior under similar conditions of stress and strain as those associated with scratch and mar conditions. Additionally, recent developments allow for indentation testing under conditions of dynamic oscillation, such that coupling quasi-static tests, such as the creep and relaxation tests, with the dynamic tests can be used to characterize polymer response over a large range of time/frequency.

In Fig. 5, two sets of LSCM images are shown which capture the damage created by scratching an epoxy sample with the rounded conical tip of radius 1.5 μm using a progressive-force test, in which the force was ramped from 20 μN to 100 mN at velocities of 2 μm/s (left) and 250 μm/s (right). The scratch distance was 1 mm, so that the scratch on the left was created over a testing time of approximately 500 s while the scratch on the right was created over a testing time of approximately 4 s. Thus, the depth of the scratch on the right would be expected to smaller because less creep-related deformation would occur compared to the scratch on the left. Indeed, the scratch width appears to be smaller for the scratch on the left, and the penetration data generated by the instrument, shown in Fig. 6a, confirms the difference in depth, where the plots on the left and right correspond to the scratches on the left and right in Fig. 5, respectively. In Fig. 6b, similar penetration depth data is shown for PMMA under the same testing conditions. In each of the plots in Fig. 6, the lower sets of curves represent the penetration depth during the scratch, whereas the upper sets of curves represent the unrecovered depth remaining just after scratching.

For both materials, the difference in penetration depth during scratching for the two scratch velocities is approximately 1.0 μm to 1.5 μm. For the epoxy, this difference in depth increases slightly with increasing scratch distance, but the majority of this difference is evident within the first 100 μm of the scratch. For the PMMA, while the depth difference is appreciable (~1.0 μm) at a scratch distance of 100 μm, this difference increases significantly with scratch distance. This result correlates with the indentation creep data (see Fig. 2a and Fig. 3a), as the PMMA creep compliance shows more time dependence (i.e., increases more appreciably with time) compared to the epoxy. An increase in compliance is equivalent to a decrease in stiffness, and thus the PMMA exhibits decreasing stiffness under contact loads with time, allowing for more time-dependent penetration compared to epoxy. The indentation creep behavior of epoxy was somewhat more dependent upon the applied force compared to PMMA. However, because the force increases with scratch distance for progressive-force scratch tests, effects of force are not discernable from time dependence. Also during a scratch test, the friction force is largely dominated by the plowing term, which is related to the build-up of material in front of the probe, and this friction force is, in turn, related to the tensile stress behind the tip that can act to cause cracking of the material. When cracking occurs, the amount of scatter in the scratch data can increase dramatically, as shown in Fig. 7 for a progressive-force test on PMMA at a rate of 10 μm/s. The cracking is evident in the LSCM image and corresponds to a particular scratch distance, force level, and depth, and these observations roughly correspond to values at which increased scatter is observed in the residual roughness along the scratch and a particular value of friction coefficient (ratio of friction force to normal force). However, the convolution of time-dependent and force- or stress-dependent effects renders such observations qualitative.

Additionally, the force level at which cracking occurs in a progressive-force scratch test has often been labeled as a critical force that is characteristic of the material. Of course, such a force level is a function of many experimental factors and not a material characteristic. In fact, material behavior, including fracture and various failure theories, is most often based on stress and/or strain. Thus, a critical force level is not likely to provide a reliable basis upon which to judge a material's scratch resistance, even in a relative sense. For example, in Fig. 7, the PMMA cracking occurred at a critical force level of between 3.5 mN and 3.9 mN depending on whether the critical force is defined based on the roughness data or on the LSCM image. Using the same

tip and scratch rate (10 μm/s), no cracking was observed in constant-force scratch tests for forces up to 4.0 mN. The scratch depths related to cracking ranged from 700 nm to 800 nm for the progressive-force tests while cracking was observed only at depths greater than 1100 nm in the constant-force tests. The friction coefficients appear to be related primarily to the scratch depths – values of 1.0 and 1.2 corresponded to cracking in the progressive-force and constant-force tests, respectively. Thus, none of these measures appear to be appropriate characteristics upon which scratch resistance could be based.

In other recent research, the influence of the indenter geometry and the non-reproducibility of the geometry of the conical indenters often used in scratch testing were found to result in a lack of reproducibility of critical force measurements from progressive-force scratch tests [35]. As discussed previously for indentation, a representative measure of strain applied by an indentation tip is directly related to the tip geometry. While the strain related to sliding contact likely differs from that for indentation, the use of strain relationships similar to Eq. (6) and Eq. (7) resulted in good correlation between strain levels at which cracking occurred under progressive-force scratching of PMMA using two conical tips with significantly different geometries [36]. Note that in this study, the critical force values for the two conical tips were inversely correlated, i.e., showed opposing trends, as a function of scratch velocity. Thus, a critical strain measurement is much more likely to be related to material properties than a critical force. However, as discussed, current representations of strain during indentation and scratch testing are not rigorously defined but, rather, are empirically based. Further for scratch testing, strain (as well as hardness) appears to be related to the contact area, which is a function of the scratch velocity due to the time-dependent recovery of the polymer. For example, at a slower scratch rate, the polymer has more time to recover and support the rear portion of the tip, while at a faster rate, the polymer doesn't recover and only the advancing portion of the tip is in contact with the sample.

In Fig. 8, a plot of scratch depth and residual depth as a function of normal force and scratch velocity for constant-force scratch tests is shown for PMMA and the rounded conical tip of radius 1.0 μm. The lack of variation in the applied force allows the time-dependant behavior to be explored. In this figure, both the penetration during scratch and the depth of the deformation remaining just after the scratch increased with increasing force and decreasing scratch velocity. Friction coefficient (data not shown) also was larger at slower velocities but with no discernable dependence on force within this small range. Also, as the force was incrementally increased from 3.8 mN to 4.1 mN, the damage mechanisms change from nonlinear viscoelastic or viscoplastic behavior to fracture. Further, cracking was observed at a force of 4.0 mN and velocities of 1 μm/s and 10 μm/s but not at 100 μm/s. Thus, the results of the progressive- force and constant-force scratch tests indicate that the viscoelastic behavior of the polymer influences the stresses and strains through the time-dependent penetration, the build-up of material ahead of the scratch probe, and the recovery of material behind the scratch probe, all of which are important factors that determine the states of stress and strain and the resulting surface and sub-surface damage.

Because scratch and mar resistance is a performance attribute, statistical aspects related to the anticipated set of service conditions must be taken into account. The minimization of energy dissipation during a scratch event dictates how the deformation develops based on the relative energies of potential dissipation processes in the contact area [9]. Thus, the resulting

deformation will be related to the local polymer structure and properties and the distributions of forces, rates, temperatures, particle sizes, and other service variables that the material encounters. Use of a combined experimental and modeling approach to adequately characterize the polymer constitutive behavior, capturing the relevant time/rate, stress/strain, and temperature dependences, and approximating this behavior in a numerical model using nonlinear viscoelastic or viscoelastic-viscoplastic representations (for example, see Ref. 37). Scratch testing can then be used to verify the model under the limited range of experimental conditions available for a given apparatus. Such verification will require knowledge of the three-dimensional geometry of the tip, such as that produced by imaging the tip using atomic force microscopy [28], relative to the scratch direction, along with precisely controlled and measured forces and displacements in the normal and sliding directions. The resulting model can be used to design appropriate experiments and predict behavior under sliding contact conditions that produce scratch and mar damage, which can then be related to changes in appearance. This approach is the subject of current research at the National Institute of Standards and Technology.

IV. SUMMARY AND CONCLUSIONS

Instrumented indentation was used to measure the viscoelastic behavior of epoxy and poly(methyl methacrylate) or PMMA. Values for creep compliance and stress relaxation modulus were calculated from quasi-static indentation testing using on a model of contact between a rigid probe and a viscoelastic material. Scratch testing was performed with the same instrument on the same materials with various indentation tips under a variety of conditions. Normal and lateral forces and displacements were measured continuously, and profiles of the surface after scratching were used along with confocal microscopy to characterize the resulting deformation. The progressive-force scratch test, in which the force is increased linearly with scratch distance, was found to provide only qualitative information regarding the characterization of scratch resistance due to the convolution of time-dependent and force- or stress-dependent effects. The use of a critical force as a material characteristic related to scratch resistance is discouraged based on its dependence on multiple test variables and material properties. A critical strain value appears to be a promising alternative. However, more rigorous relationships for stress and strain are required for scratch testing, including links between strain, scratch velocity, and time-dependent recovery of the polymer. Relationships between viscoelastic behavior, scratch damage and appearance are currently being explored using experimental and modeling methods.

Acknowledgements

The authors gratefully acknowledge funding support from the NIST-Industry Consortium on Polymer Interphases. MRV also acknowledges fruitful collaborations with John Villarrubia of NIST regarding tip shape determination and Xiaohong Gu of the University of Missouri – Kansas City for epoxy sample preparation.

References

1. Betz P and Bartelt A, "Scratch Resistant Clear Coats: Development of New Testing Methods for Improved Coatings," *Progress In Organic Coatings* **22**, 27-37 (1993).
2. ASTM Committee D-1, "D 6279: Test Method for Rub Abrasion Mar Resistance of High Gloss Coatings," in Annual Book of ASTM Standards **6**, American Society for Testing and Materials, West Conshohocken, PA (1998).
3. Ryntz RA, Abell BD, Pollano GM, Nguyen LH, and Shen WC, "Scratch resistance behavior of model coating systems," *Journal of Coatings Technology* **72**(904), 47-53 (2000).
4. Courter JL and Kamenetzky EA, "Micro- and nano-indentation and scratching for evaluating the mar resistance of automotive clearcoats," *European Coatings Journal* **7**, 24-38 (1999).
5. Adamsons K, Blackman G, Gregorovich B, Lin L, and Matheson R, "Oligomers in the evolution of automotive clearcoats: mechanical performance testing as a function of exposure," *Progress in Organic Coatings* **34**(1-4), 64-74 (1998).
6. Jardret V, Lucas BN, Oliver W, and Ramamurthy AC, "Scratch durability of automotive clear coatings: A quantitative, reliable and robust methodology," *Journal of Coatings Technology* **72**(907), 79-88 (2000).
7. ASTM Committee D-1, "D 5178: Standard Test Method for Mar Resistance of Organic Coatings," in Annual Book of ASTM Standards **6**, American Society for Testing and Materials, West Conshohocken, PA (1998).
8. Briscoe BJ, "Isolated contact stress deformations of polymers: the basis for interpreting polymer tribology," *Tribology International* **31**(1-3), 121-126 (1998).
9. Briscoe BJ, Evans PD, Pelillo E, and Sinha SK, "Scratching maps for polymers," *Wear* **200**(1-2), 137-147 (1996).
10. Briscoe BJ, Evans PD, Biswas SK, and Sinha SK, "The hardnesses of poly(methylmethacrylate)," *Tribology International* **29**(2), 93-104 (1996).
11. Briscoe BJ, Pelillo E, and Sinha SK, "Scratch hardness and deformation maps for polycarbonate and polyethylene," *Polymer Engineering and Science* **36**(24), 2996-3005 (1996).
12. Briscoe BJ, Pelillo E, and Sinha SK, "Characterisation of the scratch deformation mechanisms for poly(methylmethacrylate) using surface optical reflectivity," *Polymer International* **43**(4), 359-367 (1997).
13. Jardret V, Zahouani H, Loubet JL, and Mathia TG, "Understanding and quantification of elastic and plastic deformation during a scratch test," *Wear* **218**, 8-14 (1998).
14. Kody RS and Martin DC, "Quantitative characterization of surface deformation in polymer composites using digital image analysis," *Polymer Engineering and Science* **36**(2), 298-304 (1996).
15. Ni BY and Le Faou A, "Scratching behavior of polymer films using blunt spherical styli," *Journal of Materials Science* **31**(15), 3955-3963 (1996).
16. Chu J, Xiang C, Sue H-J, and Hollis RD, "Scratch and mar resistance of mineral-filled polypropylene materials," *Polymer Engineering and Science* **40**(4), 944-955 (2000).
17. Xiang C, Sue H-J, and Chu J, "Scratch Behavior and Material Property Relationships in Polymers," *Journal of Polymer Science Part B: Polymer Physics*, **39**(1), 47-59 (2001).
18. Consiglio R, Randall NX, Bellaton B, and von Stebut J, "The nano-scratch tester (NST) as a new tool for assessing the strength of ultrathin hard coatings and the mar resistance of polymer films," *Thin Solid Films* **332**(1-2), 151-156 (1998).

19. Lin L, Blackman GS, and Matheson RR, "Micro-mechanical characterization of mar behavior of automotive topcoats: Micro- and nano- wear of polymeric materials," *ACS Polymer Preprints* **39**(2), 1224-1225 (1998).
20. Shen WD, Jiang B, and Jones FN, "Measurement of Mar Resistance and Study of Marring Mechanisms of Polymeric Coatings with Scanning Probe Microscope," *Journal of Coatings Technology* **72**(907), 89-95 (2000).
21. Shen WD, Jiang B, and Jones FN, "Measurement of mar resistance and study of marring mechanisms of polymeric coatings with scanning probe microscope," *Journal of Coatings Technology* **72**(907), 89-95 (2000).
22. Du B, VanLandingham MR, Zhang Q, and He T, "Direct measurement of plowing friction and wear of a polymer thin film using the atomic force microscope," *Journal of Materials Research* **16**(5) 1487-1492 (2001).
23. Gregorovich BV and McGonigal PJ, "Mechanical properties of coatings needed for good scratch and mar," in Proceedings of the Advanced Coatings Technology Conference, ASM International, Materials Park, OH, 121-125 (1992).
24. Gauthier C and Schirrer R, "Time and temperature dependence of the scratch properties of poly(methylmethacrylate) surfaces," *Journal of Materials Science* **35** 2121-2130 (2000).
25. Gauthier C, Lafaye S, and Schirrer R, "Elastic recovery of a scratch in a polymeric surface: experiments and analysis," *Tribology International* **34** 469–479 (2001).
26. Hamilton GM and Goodman LE, "The stress field created by a circular sliding contact," *Journal of Applied Mechanics* **33**(2), 371-376 (1966).
27. Williams JA, "Analytical models of scratch hardness," *Tribology International* **29**(8) 675-694 (1996).
28. VanLandingham MR, Camara R, and Villarrubia JS, "Measuring tip shape for instrumented indentation using atomic force microscopy," *Journal of Materials Research*, submitted (2003).
29. VanLandingham MR, Chang NK, White CC, and Chang SH, "Viscoelastic Characterization of Polymers Using Instrumented Indentation – I. Quasi-static Testing," *Journal of Materials Research*, submitted (2003).
30. Corle TR and Kino GS, Confocal Scanning Optical Microscopy and Related Imaging Systems (Academic Press, New York 1996).
31. Ting TCT, "The Contact Stresses Between a Rigid Indenter and a Viscoelastic Half-Space," *Journal of Applied Mechanics* **33** 845 (1966).
32. Briscoe BJ, Fiori L, and Pelillo E, "Nano-indentation of Polymeric Surfaces," *Journal of Physics Part D – Applied Physics* **31** 2395-2405 (1998).
33. Shimizu S, Yanagimoto T, and Sakai M, "Pyramidal Indentation Load-Depth Curve of Viscoelastic Materials," *Journal of Materials Research* **14** 4075 (1999).
34. Tabor D, Hardness of Metals, 3rd ed. (Clarendon Press, Oxford, England 1951), pp. 8.
35. Jardret VD and Oliver WC, "On the robustness of scratch testing for thin films: The issue of tip geometry for critical load measurment", in Thin Films-Stress and Machanical Properties VIII, Materials Research Society Symposium Proceedings **594**, 395-400 (2000).
36. Jardret V and Morel P, "Viscoelastic effects on the scratch resistance of polymers: Relationship between mechanical properties and scratch properties at various temperatures," in Polymer Interfaces and Thin Films, Materials Research Society Symposium Proceedings **710**, 93-98 (2002).

37. Ovaert TC, Kim BR, and Wang J, "Multiparameter Models of the Viscoelastic/Plastic Mechanical Properties of Coatings via Combined Nanoindentation and Non-Linear Finite Element Modeling," *Progress in Organic Coatings* (2003) in press.

Figure Captions

FIG. 1: Plots of load, *P*, and displacement, *h*, as a function of time for indentation tests in which (a) creep and (b) stress relaxation behavior are measured. Data are shown for experiments on epoxy using a Berkovich pyramidal tip and the DCM system.

FIG. 2: Log-log plots of (a) creep compliance, *J(t)*, and (b) relaxation modulus, *E(t)*, as a function of time, *t*, for an indentation experiments on epoxy using Berkovich tips. In (a), data is shown for the DCM system and in (b), data is shown for both the XP and DCM systems along with data for a tensile rheometer. For the indentation results, each data point represents an average value from 10 experiments, and for the rheometry results, each data point represents an average of 3 experiments. Error bars represent an estimated standard deviation (k = 1).

FIG. 3: Log-log plots of (a) creep compliance, *J(t)*, and (b) relaxation modulus, *E(t)*, as a function of time, *t*, for an indentation experiments on PMMA using Berkovich tips. In (a), data is shown for the DCM system and in (b), data is shown for both the XP and DCM systems along with data for a tensile rheometer. For the indentation results, each data point represents an average value from 10 experiments, and for the rheometry results, each data point represents an average of 3 experiments. Error bars represent an estimated standard deviation (k = 1).

FIG. 4: Log-log plot of creep compliance, *J(t)*, as a function of time, *t*, comparing the indentation creep data for epoxy taken with a rounded conical tip (10 μm tip radius, 45º semi-apical angle) and a Berkovich tip. Error bars not shown for clarity.

FIG. 5: LSCM images in which the damage created by scratching an epoxy sample with a rounded conical tip of radius 1.5 μm using progressive-force tests is captured. In these tests, the force was ramped from 20 μN to 100 mN at velocities of 2 μm/s (left) and 250 μm/s (right) over a scratch distance of 1 mm.

FIG. 6: (a) Plots of penetration data generated by the indentation instrument during the progressive-force scratch tests described in Fig. 5, where the plots on the left and right correspond to the scratches on the left and right in Fig. 5, respectively; (b) plots of penetration depth data for PMMA under the same testing conditions. In each of these plots, the lower sets of curves represent the penetration depth during the scratch, whereas the upper sets of curves represent the unrecovered depth remaining just after scratching.

FIG. 7: An LSCM image and corresponding plots of residual roughness and friction coefficient as a function of scratch distance for a progressive-force test on PMMA using a scratch velocity of 10 μm/s. A determination of critical force values can be made from either the LSCM image or from the residual roughness level, where evidence of cracking in the LSCM image or increased scatter in the residual roughness data corresponds to a particular scratch distance, force level, and depth.

FIG. 8: Plot of scratch depth and residual depth as a function of normal force and scratch velocity for constant-force scratch tests. Each data point represents an average value from a minimum of 3 experiments, and error bars represent an estimated standard deviation (k = 1).

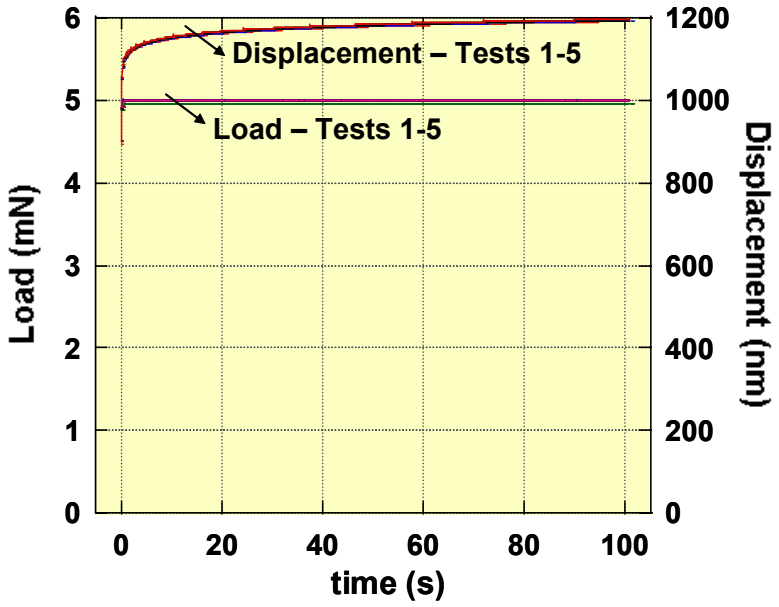

(a)

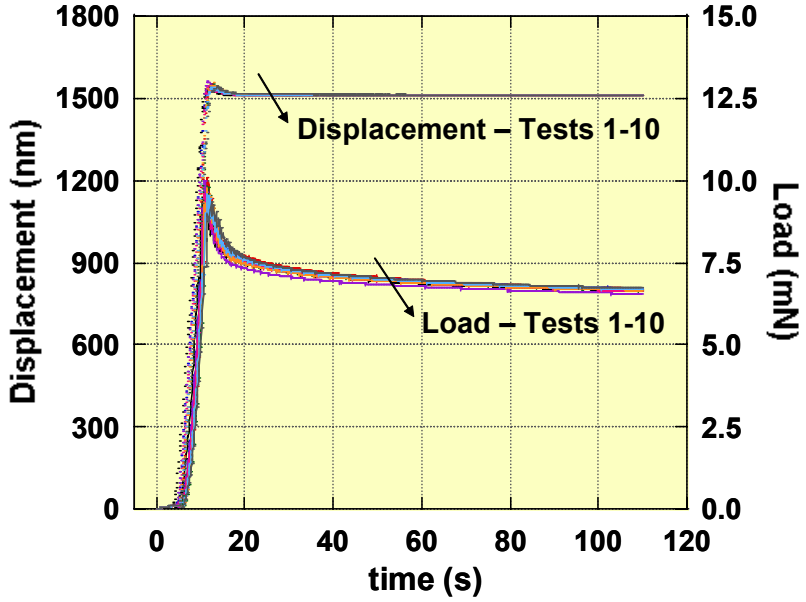

(b)

FIG. 1 VanLandingham et al.

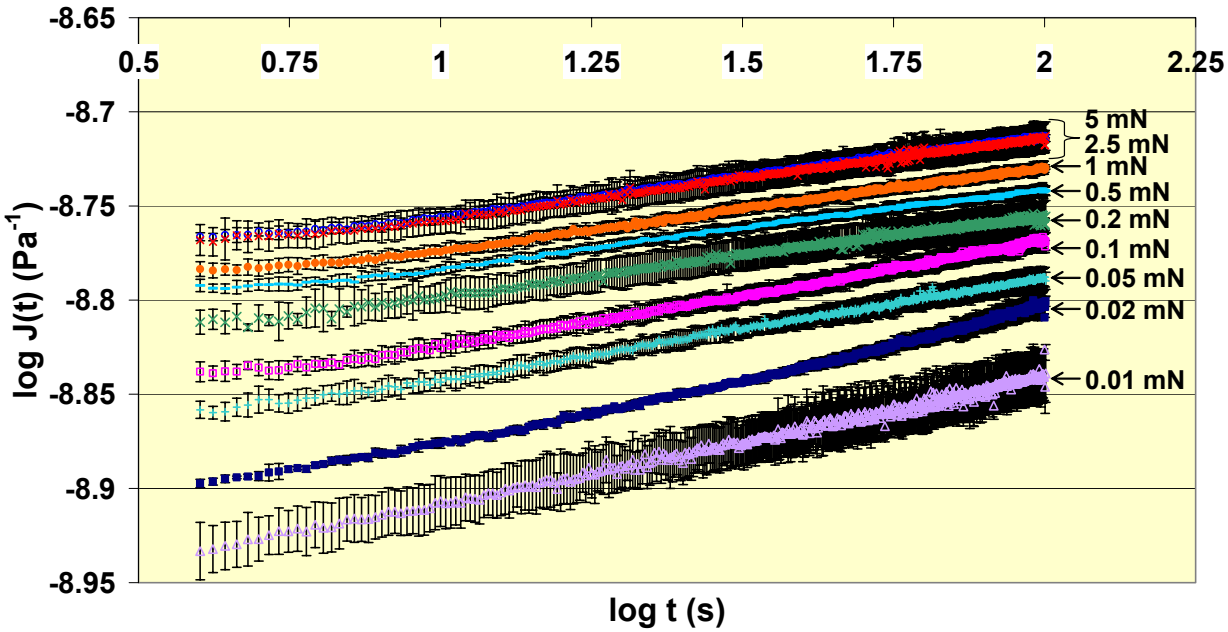

(a)

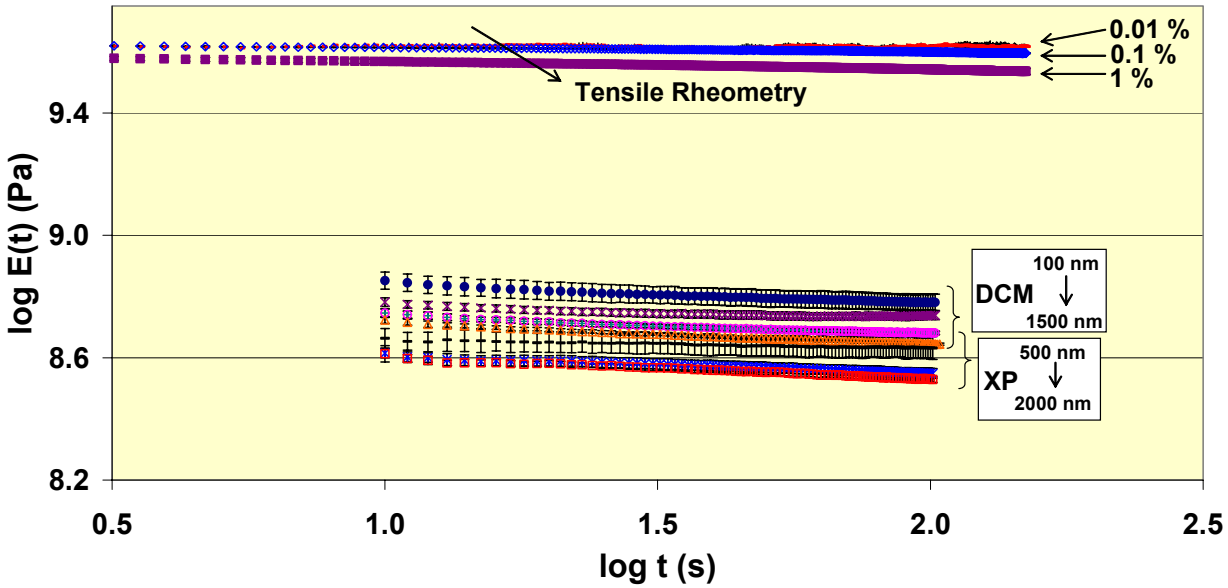

(b)

FIG. 2 VanLandingham et al.

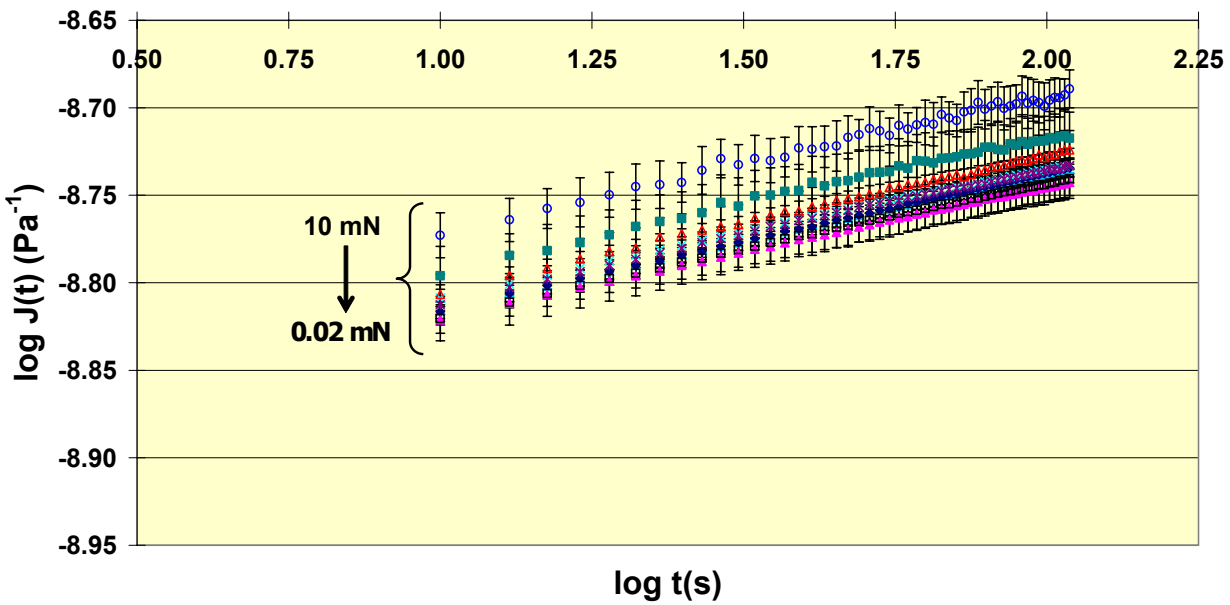

(a)

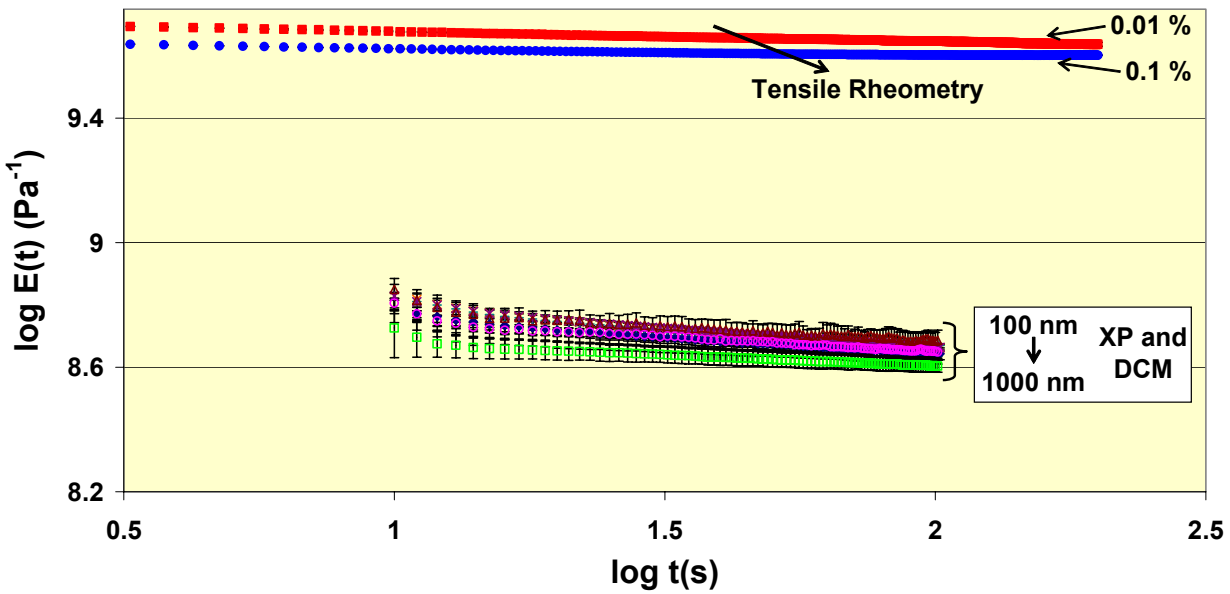

(b)

FIG. 3 VanLandingham et al.

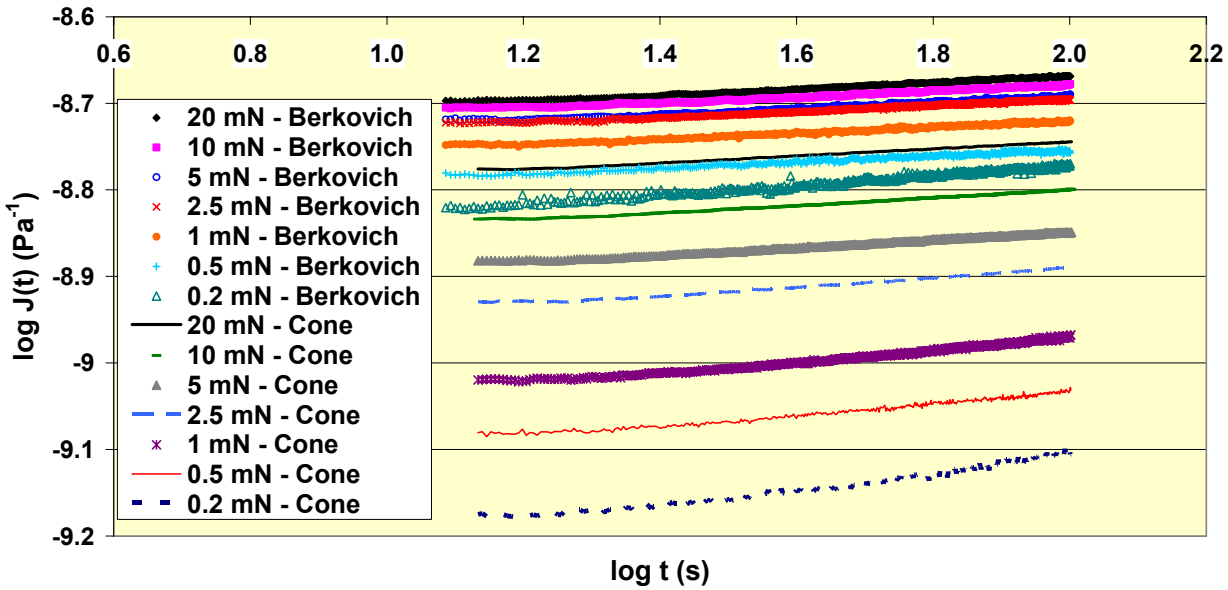

(a)

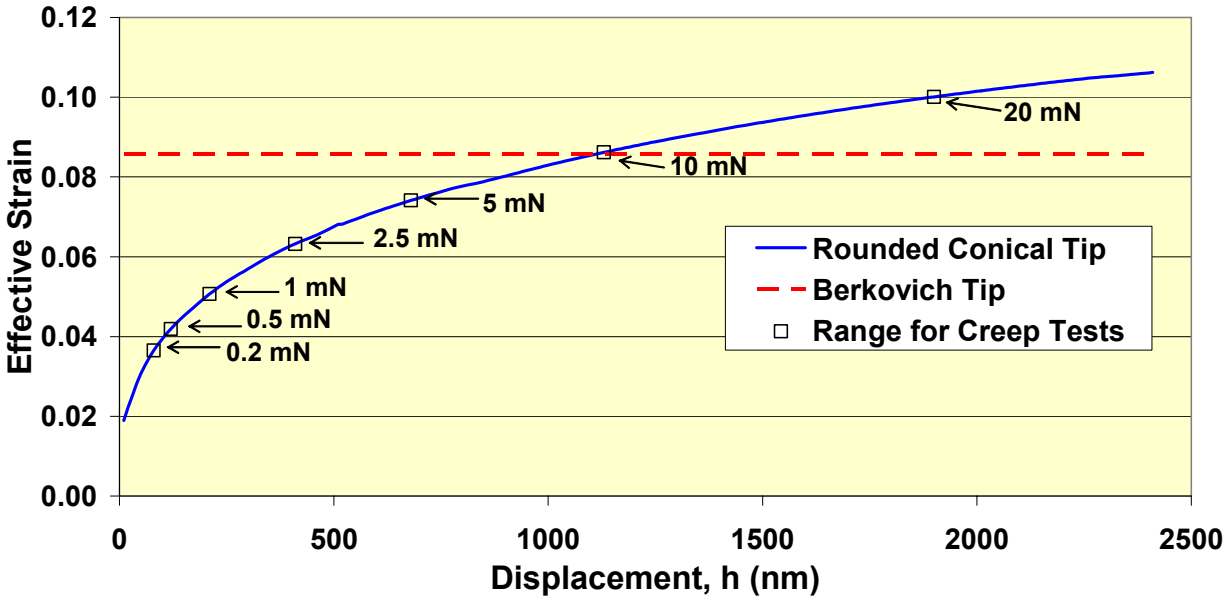

(b)

FIG. 4 VanLandingham et al.

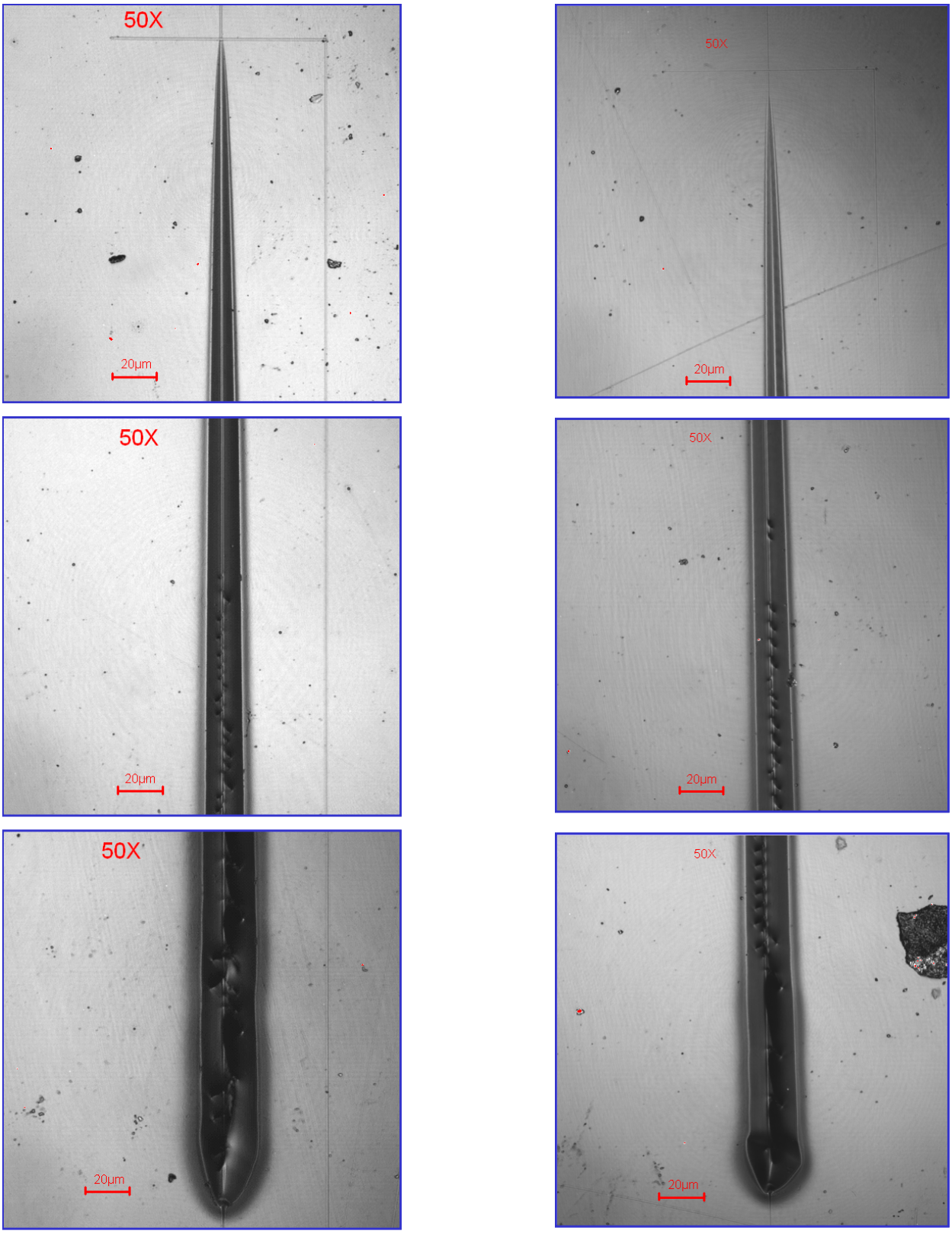

FIG. 5 VanLandingham et al.

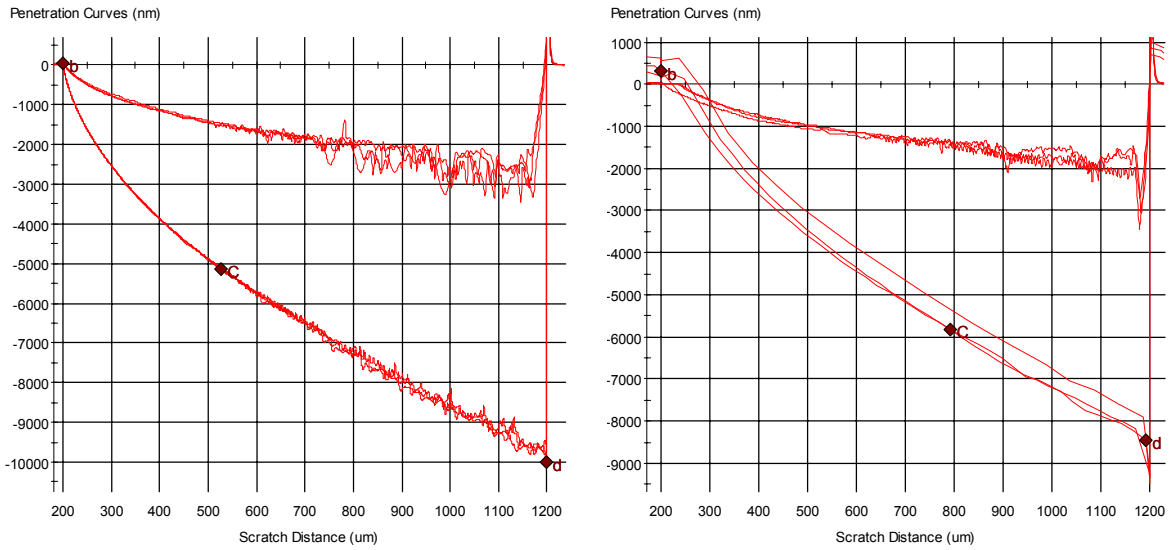

(a)

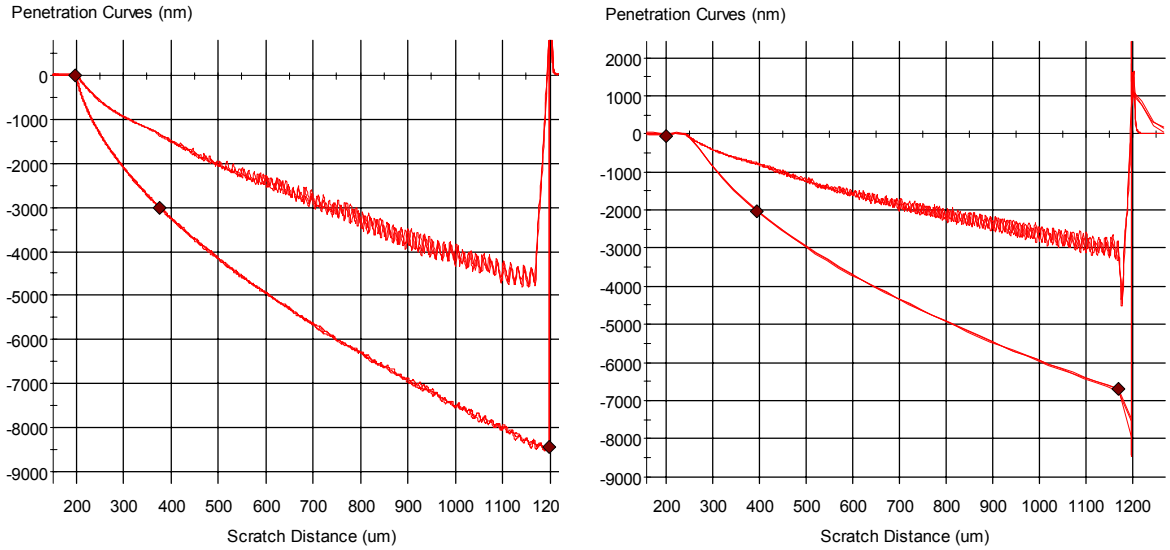

(b)

FIG. 6 VanLandingham et al.

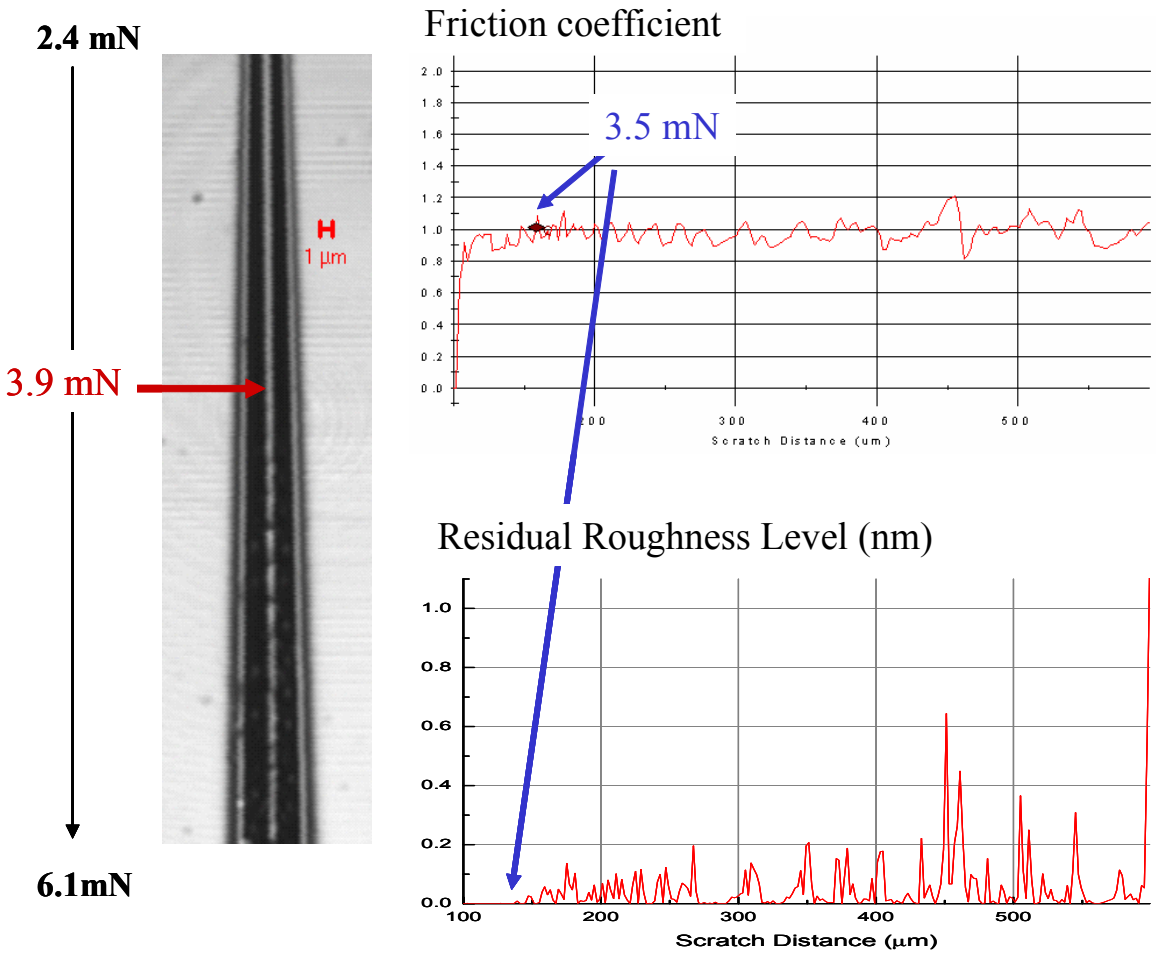

FIG. 7 VanLandingham et al.

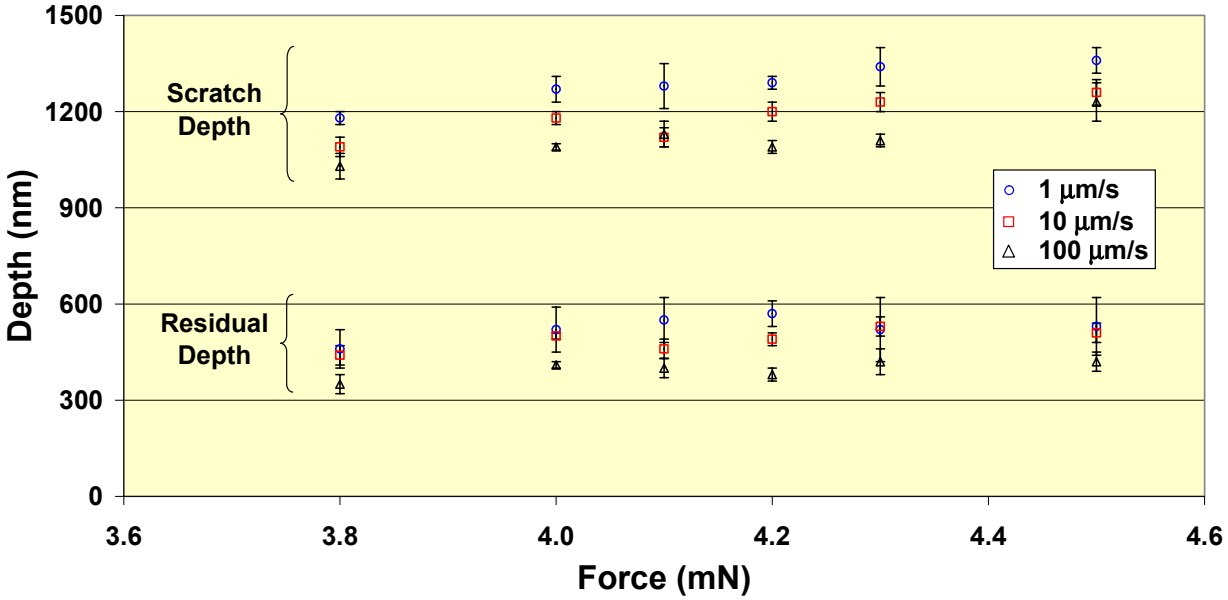

FIG. 8 VanLandingham et al.